JOURNAL OF MATERIALS SCIENCE 13 (1978) 1061–1074

# The effect of electron beam welding on various properties of three austenitic stainless steels

G. D. RAASCH, Z. A. MUNIR
*Materials and Devices Research Group and the Department of Mechanical Engineering, University of California, Davis, California 95616, USA*

The influence of electron beam welding on various properties of semistable austenitic stainless steels: 304L, 316 (low nitrogen), and 21-6-9 were investigated. Tensile tests performed on transverse butt joints gave joint efficiences approaching 95% of theoretical efficiencies. The joint ductility for all steels, however, was 50 to 70% that of unwelded samples. Hardness testing revealed that the parent matrix was harder than the heat affected zone (HAZ) which in turn was harder than the fusion zone. Microstructural examination showed that the residual 11% cold-working had induced a partial martensitic transformation in the HAZ. The formation of $(Fe, Cr)_{23}(C, N)_6$ precipitate is responsible for the observed change in mechanical properties in the fusion zone. Electron microprobe analysis showed that a redistribution of the metallic elements (Ni, Cr, Mo) occurred in the fusion zone but that the nonmetals (P, S, Si) were relatively unaffected by the fusion process. Corrosion sensitivity tests showed that only the 304L steel was susceptible to corrosion cracking. Microstructural observations of failed surfaces of this steel reveal that fracture begins in a semi-brittle mode at the weld root and continues through the HAZ in a ductile manner.

## 1. Introduction

There has been considerable interest in the effects of welding austenitic stainless steels from a materials point of view. Zemzin *et al.* [1] performed bend tests on welded joints of several austenitic stainless steels to determine the sensitivity to brittle fracture and found that alloys with 2% Mo showed the best resistance to fracture in the heat affected zone (HAZ). Lepsatre *et al.* [2] studied the weldability of 18% Cr–10% Ni austenitic steels with a nitrogen range of 0.1%–0.2% and Arrata *et al.* [3] investigated the influence of nitrogen on the mechanical properties of welded austenitic stainless steels. The latter authors found that the crack susceptibility for welds follows the order: 304L > 321 > 304 > 316 > 316L > 310S. It also was noted that 4 to 5% δ-ferrite helps lower crack susceptibility, while an increase in the nitrogen content increases the susceptibility. Increased ferrite contents not only decrease the formation of cracks but also reduce the sensitivity of the steel to grain boundary corrosion [4]. Bernstein [5] examined the effects of sulfur and phosphorus as impurities in the welds of austenitic stainless steels. It was pointed out that current specifications for the contents of these impurities is too high and suggested using extra-low carbon stainless steel to ensure adequate mechanical properties after welding. Parfessa *et al.* [6] found that sulfide films formed on boundaries between primary and secondary structures in an 18% Cr–8% Ni austenitic steel. Microcracks were found to be initiated from these films on ferrite boundaries.

While considerable interest in the electron beam weldability of numerous alloy steels has been shown [7–13] little interest in the weldability of austenitic stainless steels has been exhibited [14–16] particularly in investigating the effects of the various material parameters [17]. Brooks [17]

TABLE I Chemical analysis of steels

| Steel | Composition (wt %) | | | | | | | | | | |
|---|---|---|---|---|---|---|---|---|---|---|---|
| | C | Mn | Si | P | S | Cr | Ni | Mo | Cu | N | Fe |
| 304L | 0.026 | 1.52 | 0.69 | 0.04 | 0.07 | 18.40 | 10.40 | 0.25 | 0.21 | 0.28 | Balance |
| 316 | 0.040 | – | 0.10 | 0.013 | 0.005 | 17.60 | 13.62 | 2.46 | – | 0.047 | Balance |
| 21-6-9 | 0.019 | 9.46 | 0.15 | 0.004 | 0.003 | 19.75 | 7.16 | 0.15 | 0.20 | 0.28 | Balance |

found a close correlation between the electron beam weldability and the nitrogen content of the steel. As the nitrogen content was increased the quality of the weld decreased. He also observed that both nitrogen and manganese were lost by volatilization during the welding process, but made no attempt to relate this to the mechanical properties of the welded material.

Clearly there is a need for an investigation of the effects of certain impurities on the welding of austenitic stainless steels. The effects of individual impurities in austenitic stainless steels are well-documented [18–22] as well as the individual effects on the properties of the weld [1–6]. There has been considerable interest, but very little work done, in defining a weldability limit through specifying optimum alloy contents and minimum impurity levels. The purpose of this work is to determine some of the interdependent relationships between weldability, as determined by the mechanical properties, and the contents of the major and minor components of austenitic stainless steels.

## 2. Experimental materials and methods

Austenitic stainless steels 304L, 316, and 21-6-9 were investigated. The 304L was obtained from G. O. Carlson Inc., in sheets measuring 61 cm × 89 cm × 4.5 cm. It was cross-rolled to 2.3 cm, annealed, quenched, pickled, and cross-rolled to 2.0 cm producing a 10 to 12% cold-working. The 316 steel was supplied by Latrobe Steel Co., Latrobe, Pennsylvania as a 12.4 cm diameter bar. The forging process followed a forming series of cylinder to short fat cylinder to cube to octahedron and back to cylinder. It was cross-rolled to 2.3 cm, annealed, quenched, and pickled. The steel was finally cross-rolled to 2.0 cm producing 10 to 12% cold-working. The 21-6-9 steel was obtained from Carpenter Technology, Reading, Pennsylvania as a 23 cm × 23 cm × 117 cm billet. The forging process followed a forming series identical to the 316, finishing with a plate 2.0 cm thick with 10 to 12% cold-working. A chemical analysis for these steels is given in Table I. It should be noted that the 316 steel has a low nitrogen content.

The plates, 2.0 cm thick, were cut into welding specimens of 5.1 cm × 15.2 cm × 2.0 cm, or 10.2 cm × 15.2 cm × 2.0 cm, depending on their intended use. The larger specimens were used solely for tensile testing samples. All other tests were performed on the smaller samples. Welding was performed on a Brad Thompson Industries electron beam welder. All samples were welded along the centre line for approximately 10.2 cm. This produced a confined weld which developed higher residual stresses upon welding than an unconfined type weld. The welds were produced with a 24.5 kV accelerating voltage and approximately 100 mA welding current. The beam was focused at a plane 0.16 cm below the upper surface of the specimen. The welding speed was roughly 276 cm $min^{-1}$ but this was continually adjusted by the operator to provide a weld of optimum depth. All welds had a penetration of at least 1.8 cm. The background pressure of residual gases was less than $6.66 \times 10^{-9}$ MPa for all welding operations. The specimens were water quenched 40 sec after completion of the weld. Test samples

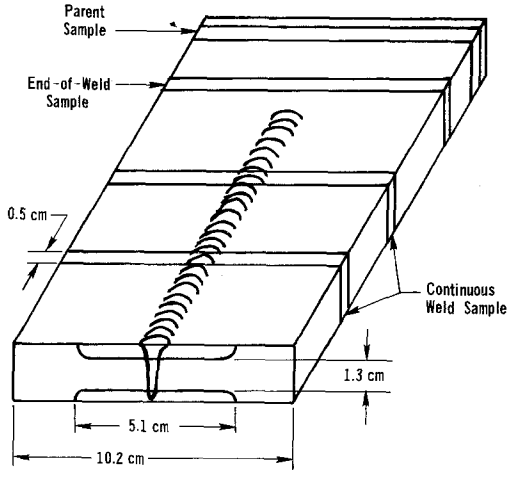


*Figure 1* Schema of tensile specimen and preparation.

were cut from the welded specimens on a 25.4 cm Buehler 1030 cut-off wheel. Three primary regions of the welded specimens shown in Fig. 1 were studied for testing purposes: continuous weld, end-of-weld, and parent material (no weld). A series of mechanical tests and several different examinations were performed on samples taken from these three regions.

Tensile specimens were machined from weld samples as shown in Fig. 1. The gauge dimensions for the testing were 5.1 cm x 1.3 cm x 0.5 cm. Tensile testing was performed at 0.25 cm $min^{-1}$ cross-head speed on an Instron tensile testing machine with a Gr 9072 Kg load cell.

Hardness specimens were surface finished on a Buehler Surfimet Grinder 16-1255 to $Al_2O_3$ 400 grit. A light etch was made to determine the centre of the weld in the cross-sectioned samples. Hardness readings were taken on a Wilson Rockwell Hardness Tester model 3JR at intervals of 0.32 cm for 1.9 cm on each side of the weld.

An Applied Research Laboratories electron microprobe analyser was used to determine the concentrations of iron, chromium, molybdenum, silicon, sulfur, and phosphorus at 10 $\mu$m increments along a path traversing the weld, HAZ, and portions of the parent material. A continuous scan was also employed to supply additional information that the step scan could not produce. The electron beam scans from the unaffected region, through the HAZ, to the weld, and continuing through the HAZ to the unaffected region were made at a rate of 196 $\mu$m $min^{-1}$. The output of the electron microprobe was connected to a Hewlett–Packard 7030A Autograph $X$–$Y$ Plotter. This provided a continuous picture of the relative fluctuations in composition of the different elements as a function of position. The electron microprobe was also used in a backscatter analysis. A region 200 $\mu$m by 300 $\mu$m was scanned by the electron beam and specific wavelength backscatters were recorded on a Polaroid film producing a "picture" of the variations in concentration of a given element in a given area.

For microstructural analysis specimens were cut and ground through $Al_2O_3$ 600 grit. They were then polished on a Buehler Polishing Wheel with 6 $\mu$m, 1 $\mu$m, and finally, with $\frac{1}{4}$ $\mu$m diamond paste. An electrochemical etch solution was prepared with 10 g of oxalic acid and 100 ml of water. Samples were etched for one minute at 7 V with a current density of about 1.5 A $cm^{-2}$. All samples were then cleaned in a soap solution in a Buehler Ultrasonic Cleaner. Etched samples were examined under magnifications from 75 x to 800 x in a Leitz–Wetzler Photomicrograph and notable features were photographed. Samples of parent, end-of-weld, and continuous weld were examined in this manner.

Samples from the three primary regions defined in Fig. 1 were cut in thicknesses of 0.64 cm and placed in a solution of 1% sodium fluoride + 20% nitric acid [23] for 2 h at room temperature. After this exposure they were bent over a mandrel with

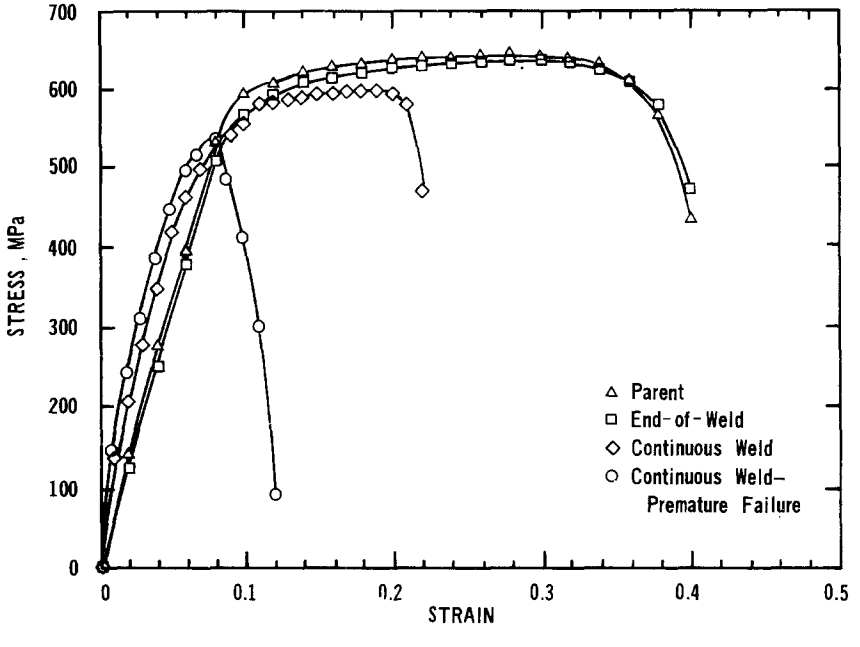


*Figure 2* Stress–strain curve for 304L stainless steel samples.

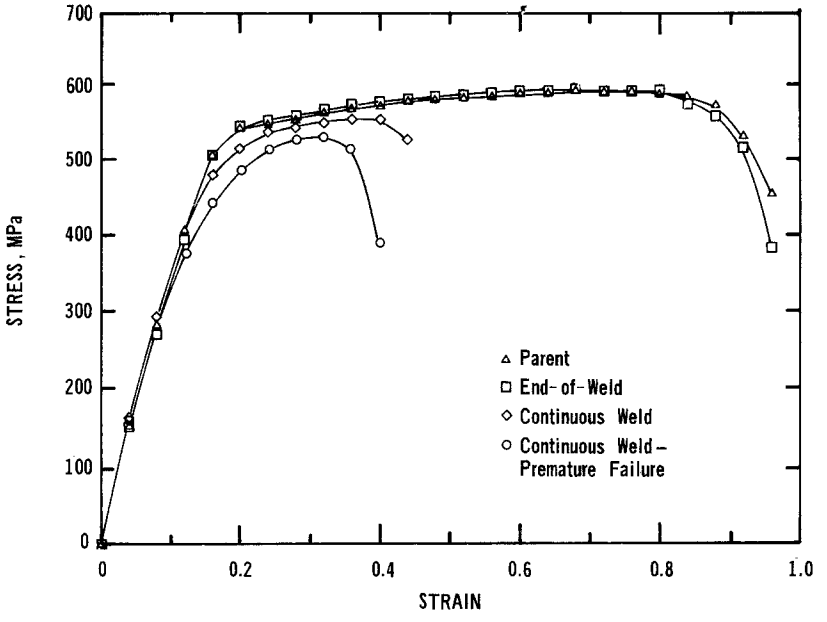


*Figure 3* Stress–strain curve for 316 stainless steel samples.

a radius equivalent to twice the thickness of the samples, 1.3 cm, and then examined visually or under a very low power binocular microscope for cracking. A Cambridge scanning electron microscope was employed to observe the surfaces of failed corrosion specimens. Magnifications of up to 5000 × were used to photograph the surface morphology.

## 3. Results

### 3.1. Tensile test

Figs. 2 to 4 are typical stress–strain curves of 304L, 316, and 21-6-9 steels, respectively. Over 44% of the 304L and 31% of the 316 continuously welded samples exhibited premature failure i.e., a characteristic failure at a tensile strength lower than theoretical with an obvious reduction in total strain. A comparison between parent, continuous weld, and end-of-weld samples is provided in each of the figures. Fig. 2 shows that the 304L continuous weld samples failed at about half the strain (0.2) of the parent and end-of-weld samples (0.4). Also shown in Fig. 2 is an example of the premature failure mode of the continuously welded samples. The continuously welded samples failed at a quarter of the total strain of the parent and

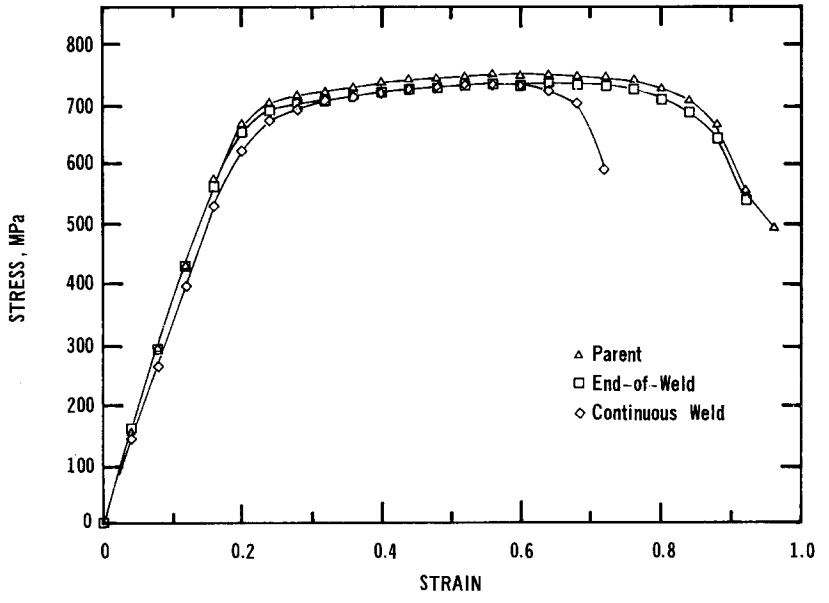


*Figure 4* Stress–strain curve for 21-6-9 steel.

end-of-weld samples. Fig. 3 provides a comparison of the typical tensile results of 316 parent, continuous weld, and end-of-weld samples. It is observed that the continuous weld samples has a tensile strength that approaches theoretical and fails at a strain (0.45) approximately half that of the theoretical value (0.95). The 316 steel also exhibited premature failures which are provided for comparison in Fig. 3. While the total strain of the continuous weld samples which failed prematurely is close to that of the normal continuous weld, the 0.2% offset yield and ultimate strengths are notably lower. Fig. 4 shows the stress–strain curve for parent, continuous weld, and end-of-weld for the 21-6-9 steel. The strain of the continuous weld (0.7) is about 75% that of theoretical (0.95). The 21-6-9 steel did not exhibit any continuous weld premature failures.

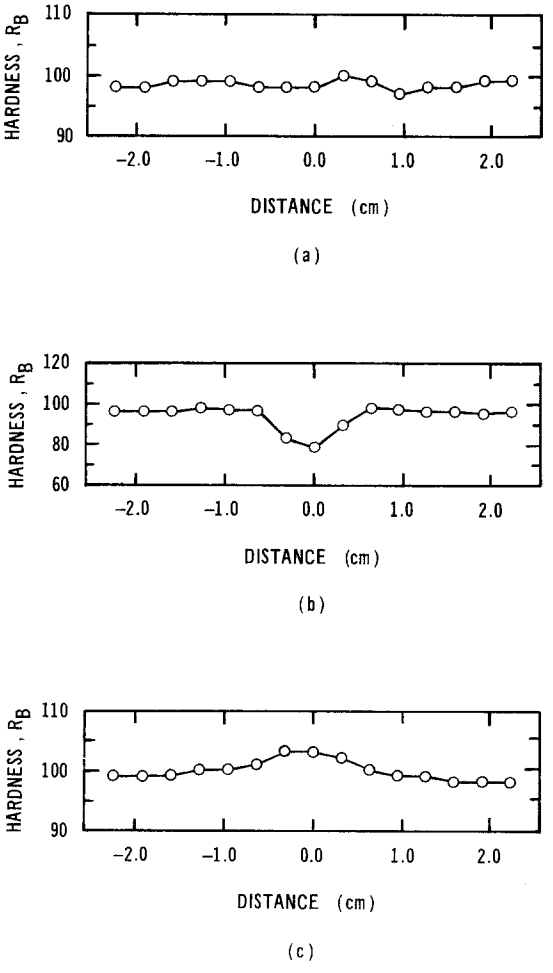


*Figure 5* Hardness profile for 304L stainless steel; (a) parent material, (b) continuous weld, (c) end-of-weld.

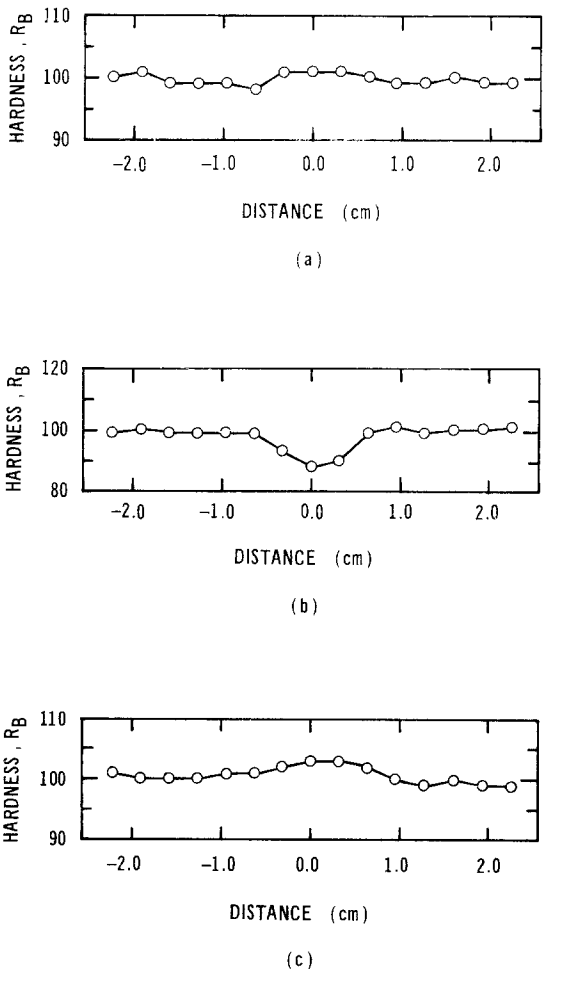


*Figure 6* Hardness profile for 316 stainless steel; (a) parent material, (b) continuous weld, (c) end-of-weld.

## 3.2. Hardness test

The Rockwell B, $R_B$, hardness data are plotted in Figs. 5 to 7 as a function of position for the three regions of the steels investigated. Fig. 5 shows the change in hardness of the 304L parent, continuous weld, and end-of-weld samples at various distances from the centre of the fusion zone. The centre of the fusion zone is the softest and the region corresponding to the HAZ is harder than the fusion zone but is not as hard as the parent matrix. Fig. 5 also shows that there is no softening in the region associated with the end-of-weld in the 304L and that the hardness of the parent matrix can vary by as much as $4R_B$ hardness points. The hardness of the 316 continuous weld is shown in Fig. 6. Similar to the 304L, the continuous weld 316 has a parent matrix harder than the HAZ, which is harder than the fusion zone. Furthermore

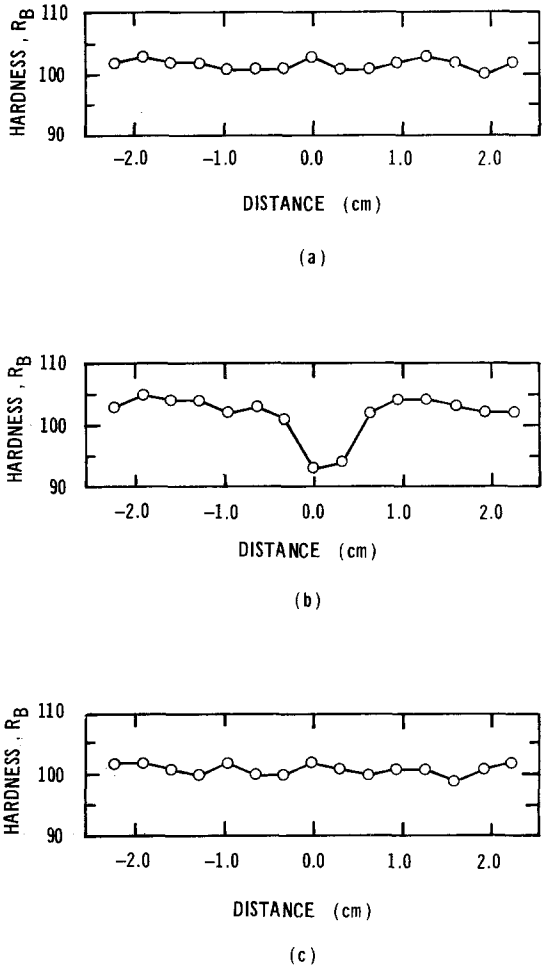


*Figure 7* Hardness profile for 21-6-9 steel; (a) parent material, (b) continuous weld, (c) end-of-weld.

it is shown that the hardness values of the end-of-weld sample and the parent sample are essentially the same. Fig. 7 shows similar changes in the hardness profiles of the three regions of samples of 21-6-9 steel. It is seen that in all steels the HAZ was softer than the parent matrix and the fusion zone was softer than the HAZ. The end-of-weld samples showed no statistically significant changes in hardness.

### 3.3. Electron microprobe

Continuous scan electron microprobe analysis for the three different continuously welded steels included the elements chromium, nickel, manganese, molybdenum, sulfur, phosphorus, and silicon. Analysis of the 304L, Fig. 8, shows several interesting features occurring in the fusion zone. While the average content of the nickel remains constant, the "spread" (the difference between adjacent high points and low points) is considerably larger indicating a localized segregation of the nickel in the fusion zone. Manganese, on the other hand, shows an overall decrease in concentration in the fusion zone while the trace elements Si, P, and S appear to be unaffected by the fusion process. Similarly, a continuous scan of the continuous weld sample for 316, Fig. 9, indicates that the three alloying metals Cr, Ni, and Mo experienced an increased "spread" in the fusion zone again indicating that some segregation of these elements had occurred. A large silicon inclusion was observed near the centre of the fusion zone which corresponds to the very low concentration of Cr, Ni, and Mo at that point. The content of the sulfur was not found to be dependent on the welding process. The scan of a 21-6-9 continuous weld sample showed no unusual features except for a slight nickel depletion at the HAZ–fusion zone interface. Continuous scans of the end-of-weld samples were also performed. In all three steels there are occasional random "spikes", indicating enrichments of a specific element; but there are no ordered or coordinated fluctuations indicating any atomic rearrangement at the end of the weld. Scans of parent material gave identical results to those for end-of-weld samples.

A step-scan microprobe analysis of continuously welded 304L, 316 and 21-6-9 steels were also performed. As in the case of the continuous scan the step scan shows atomic rearrangement occurring within the fusion zone as shown in Fig. 10 for the 304L steel. The step scan lacks the continuity of the continuous scan but has the advantage of precise composition measurement whereas the continuous scan only records the relative composition changes. Both types of analyses are presented to provide a more complete representation. The step-scan data reduction includes a first approximation program which subtracts the value of the background radiation from the detected radiation, and then divides that by the normalized standard radiation value for the element in question, and a correction program. The correction program was the Colby Magic IV Program [24] which corrects first approximation data for dead-time losses, background, absorption (Heinrich, Duncumb–Shields, Philibert) [25], backscatter losses (Duncumb) [25], and ionization-penetration (Philibert–Trixier) [26]. It uses the Berger–Seltzer [27] equation for the mean ionization potential. The results of the backscatter

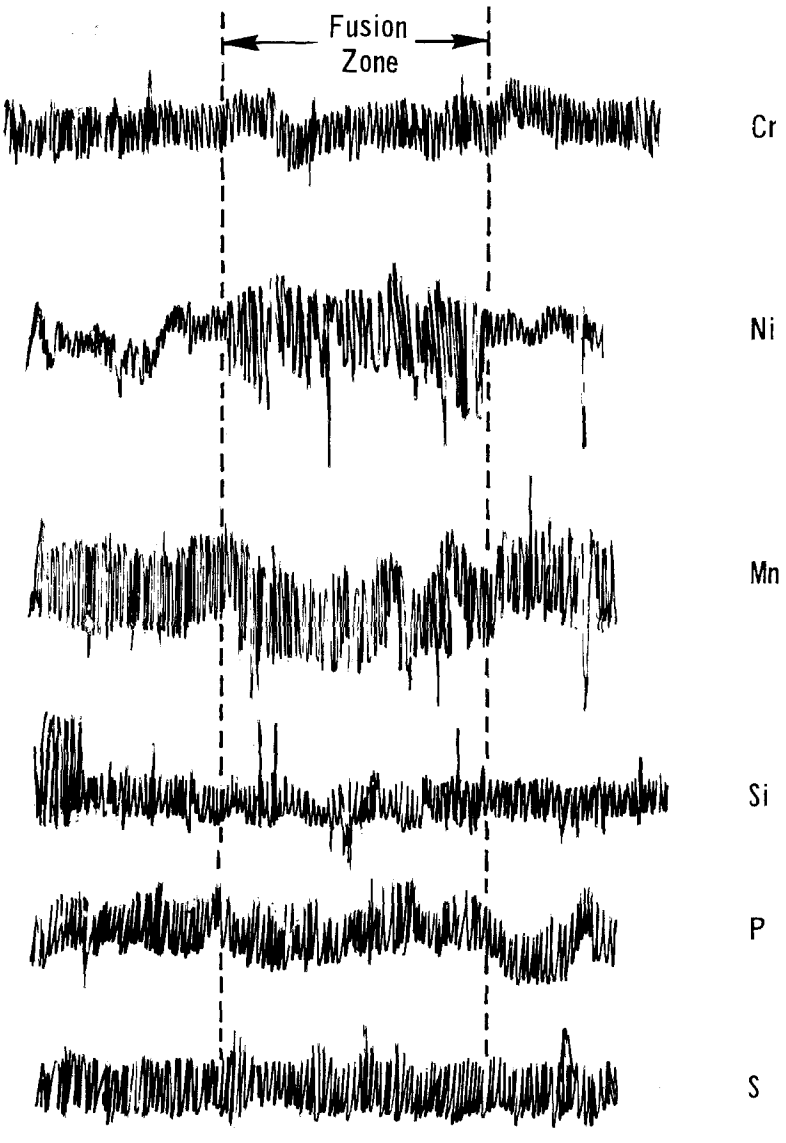


*Figure 8* Variation of concentration with position for a 304L continuous weld sample (continuous scan microprobe mode).

analysis were inconclusive. There were no observable inclusions of the minor elements (silicon, sulfur, phosphorus, manganese in the 304L and 316 steels, and Mo in the 304L and 21-6-9 steels) in the immediate area of the fusion boundary. There were also no detectable changes in the concentration of the major alloying elements (Cr, Ni, Mn in 21-6-9 and Mo in 316) across the fusion boundary.

### 3.4. Microexamination

Figs. 11a to d represent photomicrographs of 340L in the as-received and welded states. Fig. 11a shows the microstructure of the as-received 304L. The extensive banding in the grains indicates that previous cold-working induced a partial martensitic transformation. The strain-induced martensite in the parent matrix is observed in the 316 and 21-6-9 also. Figs. 11b and c show that a well-defined boundary exists between the HAZ and the fusion zone. A close examination also shows that some precipitates have formed extending from the fusion zone a small distance into the HAZ along the grain boundaries. Another interesting feature in this micrograph is the absence of the martensitic bands that were found in the parent matrix. The root of the weld or weld tip is shown in Fig. 11d. The series of parabolic bands observed in the weld root are cold shuts indicating that the melt was pulsing during the fusion process [28] instead of being smoothly continuous. A closer inspection reveals that many grains appear to continue

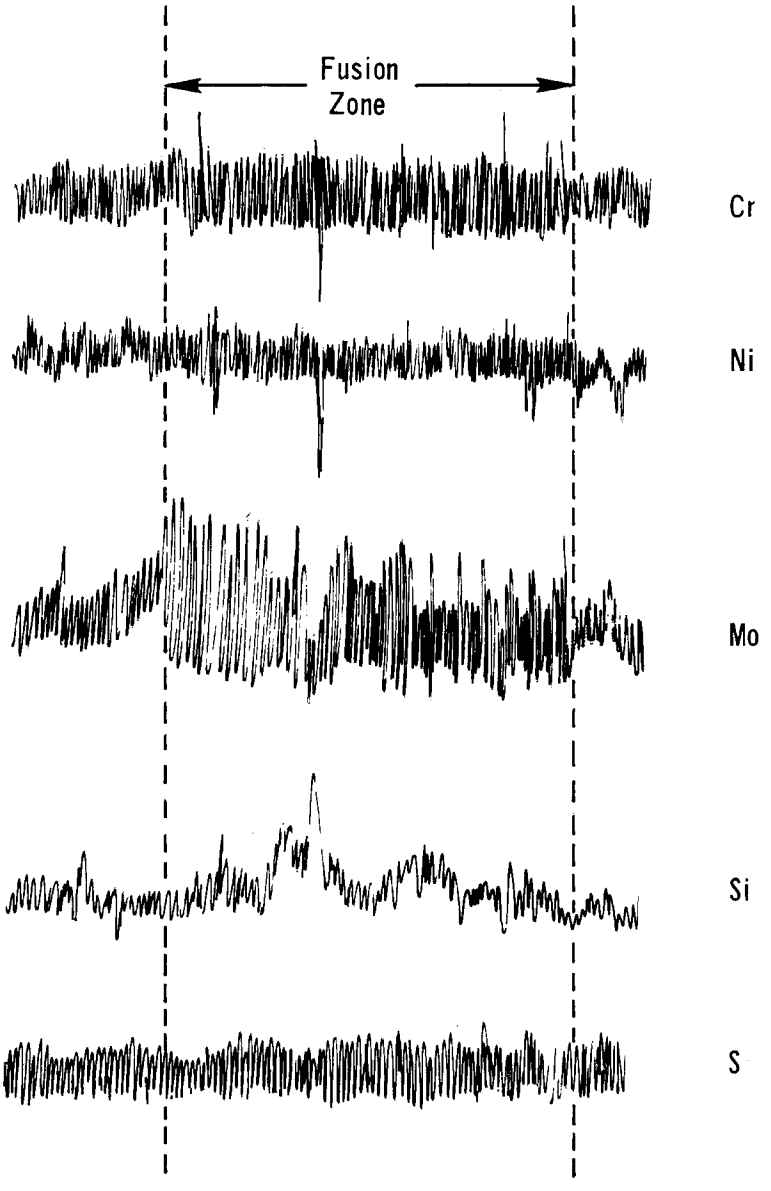


*Figure 9* Variation of concentration with position for a 316 continuous weld sample (continuous scan microprobe mode).

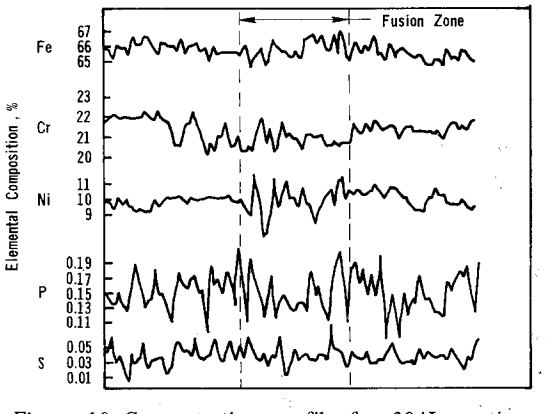


*Figure 10* Concentration profile for 304L continuous weld sample (step scan microprobe mode).

through the fusion zone boundary indicating an incomplete fusion process. No explanation can be offered for the darkened triangles which appear on the outermost cold shut.

The microstructure found in the HAZ appears to be very similar to that observed in a 304 specimen which had been sensitized (by heating at 750° C for 1 h, Fig. 12a) and subsequently annealed (by heating at 1000° C for 1 h, Fig. 12b) to dissolve the $M_{23}C_6$ precipitates. Similar observations of extensive martensitic banding in the as-received samples, the absence of such features in the HAZ, and the occurrence of cold shuts and incomplete melting at the root of the weld were also evident

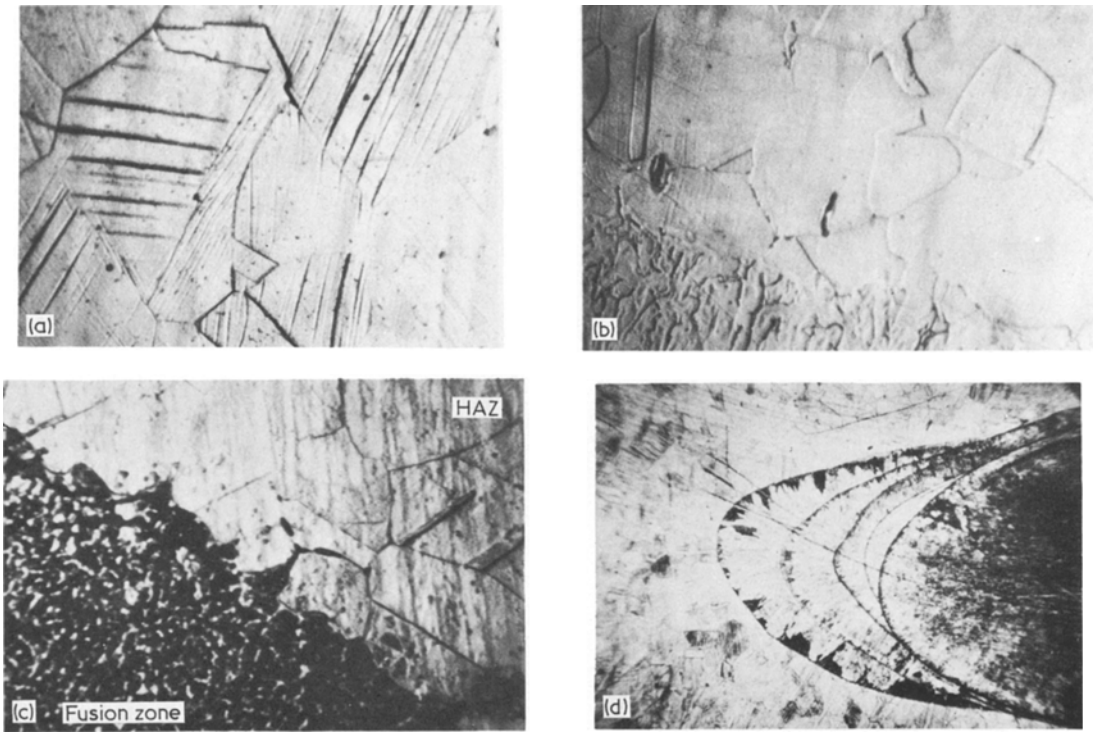


*Figure 11* Microstructural features of 304L stainless steel; (a) parent material (480 ×), (b) HAZ and fusion zone (480 ×), (c) HAZ and fusion zone (500 ×), (d) fusion root zone (46 ×).

for the 316 and 21-6-9 steels as shown in Figs. 13 and 14, respectively.

### 3.5. Corrosion sensitivity

A gravimetric method for corrosion sensitivity measurement is considered unsuitable for welded specimens where the attack is normally restricted to the HAZ. Therefore a bend test must be employed. The 304L continuous weld sample was severely attacked as was evidenced by the formation of large cracks. Both the end-of-weld and the parent 304L showed mild sensitivity to the test. The results of the corrosion sensitivity testing for the 316 and the 21-6-9 showed only mild attack on parent, continuous weld, and end-of-weld in both cases. Scanning electron photomicrographs taken of the fracture surface of the 304L corrosion sample show that failure began in a brittle mode, Fig. 15a, and continued in a ductile manner shown by the characteristic dimples, Fig. 15b.

## 4. Discussion

An examination of the results of the hardness tests shows that the HAZ in all steels was consistently softer than the parent matrix. The fusion process

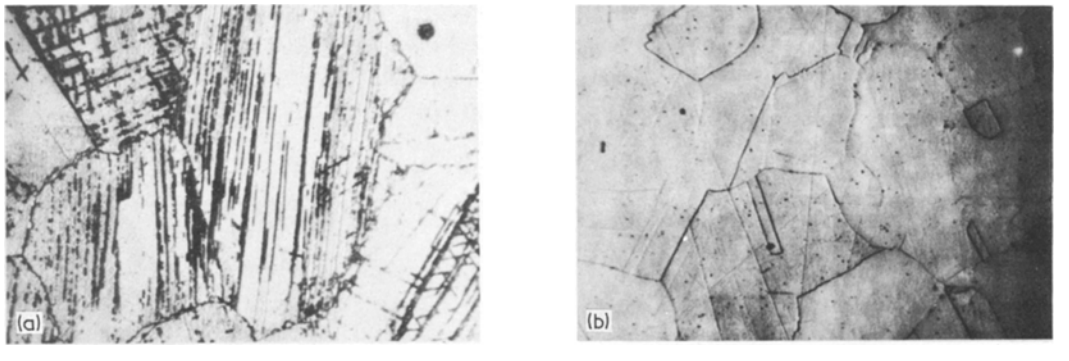


*Figure 12* Microstructural features of 304L parent sample; (a) sensitized (480 ×), (b) annealed (480 ×).

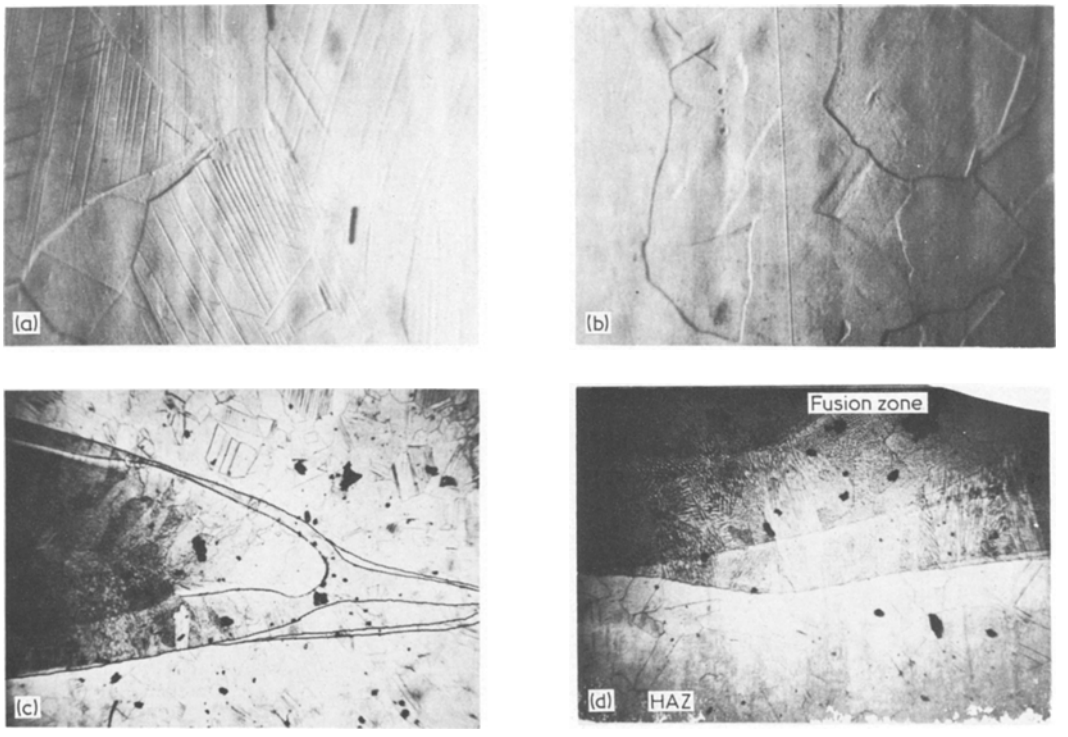


*Figure 13* Microstructural features of 316 stainless steel; (a) parent material (480 ×), (b) HAZ (480 ×), (c) fusion root zone (45 ×), (d) HAZ and fusion root zone (84 ×).

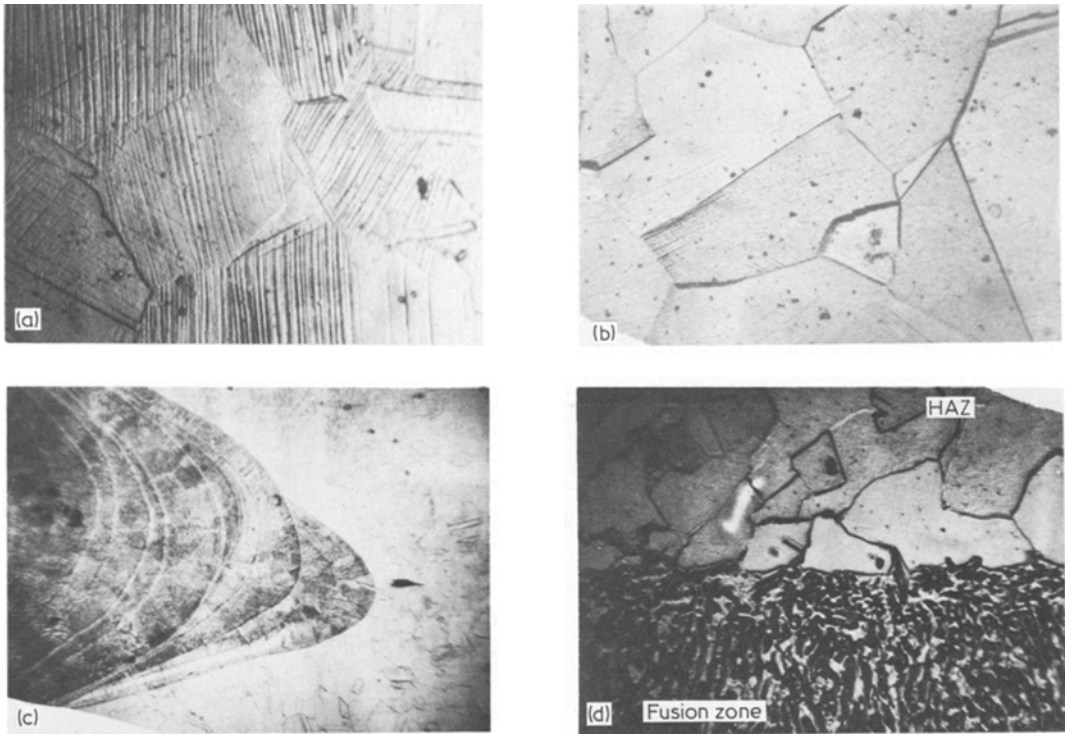


*Figure 14* Microstructural features of 21-6-9 steel; (a) parent material (480 ×), (b) HAZ (480 ×), (c) fusion root zone (46 ×), (d) HAZ and fusion root zone (480 ×).

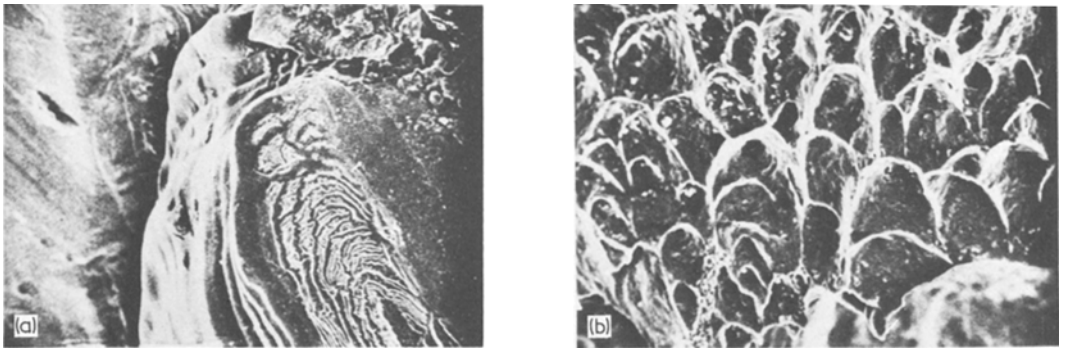

*Figure 15* Scanning electron micrographs of fracture surfaces of 304L stainless steel following the corrosion test (1200 ×).

produces enough heat to anneal the cold-work and retransform the partially martensitic matrix back to an austenitic matrix. Thomas and Kraus [29] found that the martensite to austenite formation occurs at 760° C. The temperature of the fusion zone is considerably higher (approximately 2100° C) ensuring that the transformation will take place locally before the welded sample is water quenched. The centre of the weld was found to be much softer than either the parent matrix or the HAZ in all the steels. The primary reason for this sharp decrease in hardness is that during the welding process both carbon and nitrogen are removed from the matrix and form nitrides ($z$-phase $M_zN$) and carbonitrides [$M_{23}(C, N)_6$] [19]. If the fusion zone temperature remains in the range of 500 to 800° C after welding for more than a few seconds the formation of chromium carbonitrides is thermodynamically very favourable. At this temperature the carbon and nitrogen atoms have sufficient mobility to ensure a complete reaction. This produces a fusion zone composed of $(Fe, Cr)_{23}(C, N)_6$ precipitates in a very low-carbon, high-nickel, $\delta$-ferrite matrix [4]. The effects of changes in composition on the hardness of an austenitic stainless steel are well documented [18]. Assuming that all the carbon and nitrogen were tied up in precipitates, the hardness (in $R_B$) in tne fusion zone would be 26 points lower due only to the change in these two elements. This difference of $26 R_B$ hardness points is close to the actual observed change in hardness. The change in hardness in the fusion zone in the 316 is not as large as in the 304L. While the 316 has a slightly higher carbon content (0.040%), the nitrogen level is much lower (0.047%), which offsets the increased hardness effects due to the additional carbon content. Similarly, the 21-6-9 steel did not show as great a change in hardness in the fusion zone as did the 304L. While the nitrogen content of the 21-6-9 steel was approximately the same as that of the 304L, the carbon content was lower, thus producing less change in hardness when the carbon was tied up in precipitates following the fusion process.

The results of the tensile testing showed that almost one-half (44%) of the 304L continuously welded samples and nearly one-third (31%) of the 316 continuously welded samples displayed premature failure as compared to the remainder of the continuously welded steels tested. The 21-6-9 tensile test specimens showed that there was not a single premature failure out of the 16 continuously welded samples tested. The 304L and 316 continuously welded samples failed at approximately one-half of the strain of the parent samples while the continuously welded 21-6-9 failed at 70% of the theoretical strain. Clearly the increased manganese content not only increased the tensile strength (the 21-6-9 had a 20% higher yield than the 304L or the 316) but extended the maximum strain from about 50% in parent samples of 304L or 316 to 70% in the 21-6-9. The results from the end-of-weld showed that these specimens exhibited equivalent mechanical properties to those of the parent samples. Samples from the end-of-weld were tested primarily to determine if cracks were formed by producing a confined weld situation. Microscopic examinations are very limited in scope because the probability of the surface under observation intersecting a crack that developed from a confined weld is very small. A more accurate method is to test for cracks in a volume instead of depending on discovering a crack on a randomly

selected surface. Therefore a tensile test was chosen to be the best way to determine if any pre-existing cracks were present. No evidence of pre-existing cracks was found in the parent material and all end-of-weld samples tested showed comparable results with the exception of one 304L tensile test. One sample failed after 15.2% strain as compared to about 42% for the remainder of the 304L end-of-weld samples. Additional samples were tested but no other premature failures were observed. No explanation could be offered for this singular occurrence.

The results of the microprobe analysis of the continuously welded steels showed that a very different atomic arrangement existed in the fusion zone as opposed to a region out of the fusion zone. Chromium showed very little change comparing one side of the fusion zone with the other. Nickel in all three steels and the molybdenum in the 316 displayed a dramatic change in behaviour in the fusion zone. Outside the zone, nickel and the molybdenum vary a little in composition, but the spread of the readings or the band width is relatively small. However in the fusion zone a much larger composition spread is encountered, indicating that there exist significant variations in the local compositions of these elements in this region. Austenitic stainless steels are face-centred cubic (f c c) with the major alloying elements Cr, Ni, Mo, and Mn directly substituting into the f c c matrix. After fusion has occurred and the weld is cooling $(Fe, Cr)_{23}(C, N)_6$ precipitates begin to form [30, 31]. Nickel, molybdenum, and manganese are not as thermodynamically favoured to form carbonitride precipitates as chromium and iron. Therefore as the precipitate forms it excludes nickel, molybdenum, and manganese thus producing regions of high Ni, Mo, and Mn content adjacent to precipitates (regions of low Ni, Mo, and Mn concentrations). This variation is more apparent with lower concentrations i.e., it is more severe in Mo than in Ni and more obvious in Ni than in Cr. A change in composition of 1% in Mo, representing a difference of 33% in the 316, is much more apparent than a 1% change in Ni in 304L corresponding to approximately a 10% change.

The concentration of the manganese in the 304L shows an apparent decrease in the fusion zone. The certified manganese content of the 304L is 1.52% and the observed change is only of the order of 0.1 to 0.2% difference in composition. It has been suspected by other authors that some manganese does volatilize during the welding process [17, 28]. This work on 304L supports those findings while the results of manganese vaporization in the 21-6-9 are inconclusive due to the difficulty in detecting a small change in concentration in a steel with a high manganese content. Silicon showed occasional spikes indicating that there were a few small inclusions but there seemed to be no preference for small Si inclusions to form in or out of the fusion zone. The exception was in one instance in the 316 where a very high concentration of Si in the centre of the fusion zone was observed. The peak was clipped in the graph, as were the sharp dips in the concentrations of Cr, Ni, and Mo. The inclusion might be SiC, but this conclusion is tenuous. It is obviously not a metallic precipitate due to the sharp dips in the metallic element concentrations. Both sulfur and phosphorus showed occasional, sporadic inclusions (spikes), but there was no observable change comparing the region inside the fusion zone with those out of the zone. There was no evidence to support the findings of Parfessa *et al.* [6] that sulfide films formed at boundaries between the fusion zone and the HAZ. There were no indications of sulfide films forming on fusion zone boundaries in any of the three steels as determined by continuous scan microprobe analysis, step-scan microprobe analysis, or electron backscatter analysis.

The results of the microprobe analysis at the end of the welds showed that there was no observable change occurring at any one point for all the samples. It is suspected that the temperature was too low and the time too short for atomic diffusion and rearrangement to take place. The results of the end-of-weld samples appear to support this. A continuous scan was also performed on a 316 parent sample. There was no observable difference in composition between the end-of-weld and the parent 316 steel sample.

The photomicrographs of the three austenitic steels appeared very similar in every respect. Micrographs of the parent (as-received) material all show partial martensitic transformation due to cold-working as evidenced by extensive slip systems in each individual grain. Observations of the heat-affected zone show no change in grain size but a total absence of the martensite and the slip bands that were characteristic of the parent matrix. The amount of martensite was found to gradually increase from 0% at the fusion zone

boundary, to that of the parent matrix in a distance of approximately 70 $\mu$m, the maximum width of the HAZ. In the HAZ near the fusion zone, within 100 $\mu$m, small black dots of precipitate were observed. This region received an excessive heat treatment during the welding process resulting in the formation of small regions of $M_{23}C_6$ carbides. In the micrographs showing both the HAZ and the fusion zone the grains that border the fusion zone show considerable carbide precipitation at the grain boundaries. This produces a susceptibility to intergranular corrosion. All steels displayed cold shuts at the root of the weld. This correlates with the findings of Groves and Gerken [32] which established that cold shuts, among other defects, are characteristically found in welds in steels exceeding 1.3 cm in thickness.

The photomicrograph of Fig. 11c shows the $M_{23}C_6$ particles that form on grain boundaries and $M_{23}C_6$ laths that form in the martensite regions. This surface morphology is characteristic of 18% Cr–8% Ni austenitic stainless steels that were partially transformed to martensite through cold-working and then sensitized.

The results of the corrosion sensitivity testing indicate that the 304L has been sensitized by the welding process considerably more than either the 316 or the 21-6-9 steels. This conclusion is based on the sensitization caused by the welding process, since unwelded 304L test samples performed well. Optical examination revealed that the failure consistently occurred at the fusion zone–HAZ interface. Scanning electron micrographs of the fracture surface illustrate that the fracture appeared to initiate at the root of the weld in a semi-brittle mode which continued in a ductile fracture mode [33]. Fig. 15a shows a separation of the HAZ from the fusion zone. Fracture continued in a ductile manner as revealed by the characteristically dimpled surface in Fig. 15b. This failure was only found to occur in the 304L while the other two steels tested performed satisfactorily. These findings agree with the work of Arrata *et al.* [3]. They found that the 304L had the greatest susceptibility to cracking of the six types of austenitic stainless steels tested.

## 5. Conclusions

(a) The tensile strength of the continuously welded samples of three stainless steels attained at least 90% of the theoretical strength and in some cases approached 100%. The maximum ductility was only 70% in the 21-6-9 and less than 50% in the 304L and 316 steels. Welds of 304L and the 316 steels displayed a high frequency of premature tensile test failures.

(b) The tensile strength in the end-of-weld samples was at least 98% of the theoretical value, implying that confining a weld did not produce any stress-formed cracks in the three steels investigated.

(c) The Rockwell hardness of the HAZ was lower than the parent matrix due to an austenite re-transformation and the fusion zone was softer than the HAZ because of the precipitation of the carbon and nitrogen as $(Fe, Cr)_{23}(C, N)_6$.

(d) Electron microprobe analyses showed a localized atomic rearrangement of the nickel and the molybdenum in the fusion zone with areas of enrichment adjacent to areas of depletion. The chromium content was too large to give conclusive results regarding its variation. The manganese content was found to decrease in the fusion zone and is suspected to be influenced by volatilization during the welding process. The trace elements S, P, and Si showed no observable changes in or out of the fusion zone.

(e) All steels formed cold shuts in the weld roots indicating incomplete fusion at the weld tip. Corrosion test failures in the 304L were found to originate in this region.

(f) A corrosion sensitivity test showed that only the 304L was susceptible to corrosion cracking. The fracture in the 304L fusion joints begins in a semi-brittle mode at the weld root and continues through the HAZ in a ductile manner.

## Acknowledgements

We are grateful for the interest and encouragement provided by Don Moon and Gene Stisser of the Lawrence Livermore Laboratory throughout the phases of this research. Their comments and suggestions provided a valuable input to this work. This work was supported by a grant (PO5453805) from the Lawrence Livermore Laboratory, Livermore, California.

## References

1. V. N. ZEMZIN, A. V. BOEVA and T. I. BAGRAMOV, *Automat. Weld.* **19** (1966) 1.
2. J. LEPSATRE, M. HUBERT and C. MESSAGER, *Rev. Met.* **66** (1969) 771.
3. Y. ARRATA, F. MATSUDA and S. SARUWATARI, *Trans. Japan Weld. Res. Inst.* **3** (1974) 79.

4. D. SEFERIAN, "The Metallurgy of Welding" (John Wiley and Sons, New York, 1962) p. 248.
5. A. BERNSTEIN, *Rev. Sourdure* **24** (1968) 142.
6. G. I. PARFESSA, V. V. PODGAETSKY and G. N. GORDAN, *Automat. Weld.* **18** (1965) 12.
7. O. K. NAZARENKO, V. F. GRAGIN, V. E. LOKSHIN and G. N. KORAB, *ibid* **27** (1974) 1.
8. I. Y. ZYBKO and L. V. LYUBAVSKII, *Svar. Prioz.* **5** (1970) 21.
9. A. M. MAKARA, N. E. PROTOSEI and V. G. GORGANNYI, *Automat. Weld.* **22** (1969) 81.
10. L. J. PRIVOZNIK, R. S. SMITH and J. S. HEVERLY, *Weld. J.* **8** (1971) 567.
11. P. J. KONKOL, P. M. SMITH, C. F. WILLEBRAND and L. P. CONNER, *ibid* **11** (1971) 765.
12. T. BONISZESKI and D. M. KENYON, *Brit. Weld. J.* **7** (1966) 1090.
13. A. A. WARE and E. R. FUNK, *Weld. J.* **3** (1970) 115-s.
14. H. ZURN and L. DORN, *Metall.* **21** (1967) 912.
15. N. A. OL'SHANSKY and A. V. ZAITSEVA, *Automat. Weld.* **18** (1965) 28.
16. I. Y. ZYBKO, *ibid* **26** (1973) 5.
17. J. A. BROOKS, Sandia Laboratories Report No. SLL-73-0060, Livermore, Ca., October 1973.
18. D. C. LUDWIGSON, *J. Mater.* **3** (1968) 394.
19. H. GERLACH and E. SCHMIDTMANN, *Arch. Eisenhuttenwesen* **39** (1968) 139.
20. Y. KAWABEE, R. NAKAGAWA and T. MUKOYAMA, *Trans. Nat. Res. Inst. Metals,* (Japan) **12** (1970) 57.
21. A. STEINER, *Prace. Inst. Hutniczych* **24** (1972) 255.
22. N. D. TOMASHEV, G. P. CHERNOVA and O. N. MARKOVA, *Metsniereba* (1971) 233.
23. F. CHAMPION, "Corrosion Testing Procedures" (John Wiley and Sons, New York, 1965) p. 379.
24. J. W. COLBY, "Magic IV, A Computer Program for Qualitative Electron Microprobe Analysis", Bell Telephone Laboratories (1969).
25. J. PHILIBERT and R. TRIXIER, *Brit. J. Appl. Phys.* **1** (1968) 685.
26. D. DUNCUMB and S. J. B. REED, "Quantitative Electron Probe Microanalysis,", NBS Spec. Pub. 298 (Washington D.C., 1968) p. 133.
27. M. J. BERGER and S. J. SELTZER, NASA Report N65-12506, 1964.
28. T. HASHIMOTO, F. MATSUDA and H. SUZUKI, *Trans. Nat. Res. Inst. Metals (Japan)* **7** (1965) 144.
29. S. R. THOMAS and G. KRAUSS, *Trans. Met. Soc. AIME* **239** (1967) 1136.
30. M. H. LEWIS and B. HATTERSLY, *Acta Met.* **13** (1965) 1159.
31. R. STICKLER and A. VINCKIER, *Trans. Met. Soc. AIME* **224** (1962) 1021.
32. M. T. GROVES and J. M. GERKEN, TRW Equipment Laboratories, 1969.
33. H. LIEBOWITZ, "Fracture", Vol. 1 (Academic Press, New York, 1968) p. 378.

Received 20 July and accepted 15 September 1977.